This is a preprint, the final version is subject to change, of the American Mineralogist (MSA)
Cite as Authors (Year) Title. American Mineralogist, in press.
(DOI will not work until issue is live.) DOI: http://dx.doi.org/10.2138/am-2017-5911

Quantifying and Correcting the Effects of Anisotropy in XANES Measurements of Chromium Valence in Olivine: Implications for a New Olivine Oxybarometer

Revision 1

Aaron S. Bell[1]*, Charles Shearer[1], Paul Burger[1], Minghua Ren[2], Matthew Newville[3], & Antonio Lanzirotti[3]

[1]*Institute of Meteoritics and Department of Earth and Planetary Sciences, University of New Mexico, Albuquerque, NM, 87131, USA*

[2]*Department of Geoscience, University of Nevada Las Vegas, Las Vegas, NV, 89154, USA*

[3]*University of Chicago, Centre for Advanced Radiation Sources, Chicago, IL, 60637, USA*

Abstract

Chromium valence ratios in igneous olivine may hold a wealth of redox information about the melts from which they crystallized. It has been experimentally shown that the $Cr^{2+}/\Sigma Cr$ of olivine varies systematically with fO_2, therefore measurements of Cr valence in olivine potentially be employed as a quantitative oxybarometer. *In situ* synchrotron µ-XANES analyses of Cr valence ratios of individual olivine phenocrysts in thin section have the potential to unlock this stored magmatic redox information on a fine spatial scale. However, there are still obstacles to obtaining accurate XANES measurements of cation valence in crystalline materials, as the results from these measurements can be compromised by anisotropic absorption effects related to the crystallographic orientation of the sample. Improving the accuracy of XANES measurements of Cr valence ratios in olivine by calibrating an anisotropy correction is a vital step in developing Cr valence measurements in olivine as a rigorous oxybarometer. To accomplish this goal, we have used an integrated approach that combined experiments, electron backscatter diffraction analysis, and XANES measurements in olivine to systematically examine how orientation effects the resultant Cr K-edge XANES spectra and the Cr valence ratios that are calculated from them. The dataset generated in this work was used to construct a model that mitigates the effects of anisotropy of the calculated $Cr^{2+}/\Sigma Cr$ values. The application of this correction procedure as a part of spectra processing improves the overall

accuracy of the resultant $Cr^{2+}/\Sigma Cr$ values by nearly a factor of five. The increased accuracy of the XANES measured Cr valence ratios afforded by the anisotropy correction reduces the error on calculated fO_2 values from approximately ±1.2 log units to ±0.25 log units.

INTRODUCTION

Synchrotron X-ray Absorption Near Edge Structure (XANES) measurements of the valence ratios of multivalent cations in quenched glasses and minerals are a potentially powerful tool for understanding the redox histories of magmatic rocks. Recently the experimental study of Bell et al. (2014) demonstrated that the XANES-based measurements of $Cr^{2+}/\Sigma Cr$ in olivine could potentially be employed as a sensitive indicator of magmatic oxygen fugacity. This experimental study demonstrated how synchrotron μ-XANES measurements of the Cr valence ratio in olivine could potentially be used as a method for assessing magmatic oxygen fugacity. The results of this study showed that the measured $Cr^{2+}/\Sigma Cr$ in the olivine varied systematically with the imposed experimental fO_2. The results of these experiments led the authors to suggest that Cr valence measurements in olivine combined with an experimental calibration may be exploited as a new quantitative oxybarometer for igneous rocks.

The basic principle underpinning the Cr valence in olivine (hereafter referred to as the CrViO) oxybarometer, relies on the fact that the Cr valence ratio measured in an igneous olivine is directly linked to that of the liquid from which they grew, and thus can be exploited to obtain information on magmatic oxygen fugacity. Numerous experimental partitioning studies present data suggesting that the values of $D^{ol\text{-}liq}$ for both Cr^{3+} and Cr^{2+} are nearly equivalent for basaltic magmas (Gaetani and Grove 1997, Canil 2001, and Mallmann and O'Neill 2009). The observation that olivine shows nearly the same partition affinity for either Cr2+ or Cr3+ is the reason that it is especially well situated to serve as a high fidelity mineralogical recorder of the Cr valence ratio of the liquid from which it crystallized. This point is of considerable importance, as measurements of Cr valence in olivine phenocrysts in igneous rocks can provide a unique pathway for accessing redox information about there their parental magmas, even in the absence of a quenched liquid or glassy melt inclusions.

The pioneering experiments and XANES analyses of Berry and O'Neill (2004) and Berry et al. (2006) conclusively demonstrated that the $Cr^{2+}/\sum Cr$ ratios of basaltic melts are indeed a systematic function of *f*O2, and therefore by analogy Cr valence ratios can be theoretically be utilized to calculate fO2 values in the same way that measurements of $Fe^{2+}/\sum Fe$ in a silicate melts are used for this task. It should, however, be emphasized that simply retrieving a magmatic liquid's Cr2+/∑Cr ratio via the olivine proxy is not, in of itself, a direct measure of magmatic oxygen fugacity, rather, the Cr valence ratio of the melt can be used to calculate fO_2 provided that there is a calibrated model relating Cr2+/∑Cr to fO_2, temperature, and melt composition.

Based on the framework outlined above, there is clearly much important calibration and development work that must be completed before the CrViO oxybarometer is ready to be applied to a broad range of magmatic conditions (i.e. various bulk melt compositions, temperatures, and pressures).

In addition to the calibration and experimental development work outlined in the preceding paragraphs, a perhaps even more fundamental analytical issue must be resolved before the CrViO oxybarometer can come to fruition. A significant barrier to the development of the CrViO redox sensor is the paucity of knowledge about how crystallographic orientation can affect the accuracy of XANES based measurements of $Cr^{2+}/\sum Cr$ in olivine. It has been widely recognized that XANES spectra of non-isometric crystalline materials are sensitive to the crystallographic orientation of the sample relative to the x-ray beam polarization direction. Although the majority of existing XANES anisotropy studies have primarily been focused on understanding the effects of crystallographic orientation on Fe valence measurements in amphiboles and micas (Dyar 2002 a,b, Evans et al. 2014), anisotropy is no less of a barrier to the accurate measurement of cation valences in other crystalline phases. For example, orientation effects for Cr K-edge XANES spectra in olivine have been recognized and documented by Goodrich et al. (2013). In their study of olivine from a suite of urielite meteorites, the authors showed that that the intensity of the chromium 1s-4s absorption in olivine, the spectral absorption feature used to quantify Cr valence, was significantly impacted by the crystallographic orientation of the olivine.

Changes in the spectra arising from orientation-related anisotropy, manifested as variability of the intensity of the 1s-4s absorption peaks, are a significant source of uncertainty for the calculated cation valence ratios. Therefore, the ability to clearly see past the orientation effects is a pre-requisite for the use of CrViO measurements as a robust magmatic redox sensor. In other words, to achieve the highest possible accuracy for XANES-based CrViO measurements, the effects of the olivine's crystallographic orientation must be rectified during the processing and conversion of XANES spectra into quantitative valence information.

The primary objective of this study was to investigate the Cr-XANES anisotropy in olivine and use the resultant dataset to develop corrective model to mitigate the orientation-induced errors in CrViO measurements.

EXPERIMENTAL AND ANALYTICAL METHODS

Olivine Growth Experiments

Olivine crystals used in this study were experimentally grown from CMAS (CaO-MgO-Al2O3-SiO2) liquids under controlled redox conditions. The objective of these experiments was to grow a population of randomly oriented olivine crystals from a silicate melt, with a defined $Cr^{2+}/\Sigma Cr$. The starting material for the olivine growth experiments consisted of an anorthite-diopside-forsterite mixture synthesized from reagent grade oxide powders; the composition of this mixture was $An_{40}Di_{30}Fo_{30}$ + 0.50 wt. % Cr_2O_3. (Table 1).

Olivine growth experiments were conducted in a vertical Deltech tube furnace, housed in the gas mixing laboratory at the University of New Mexico (UNM). The UNM Deltech furnace is equipped with $MoSi_2$ heating elements and a programmable, microprocessor-based Eurotherm® controller. Oxygen fugacity in the experiments was controlled with CO-CO_2 mixtures. The fO_2 values imposed by these gas mixtures were measured with a SIRO2® YSZ (Yttrium Stabilized Zirconia) electrochemical oxygen sensor. In the UNM gas mixing laboratory, oxygen fugacity is routinely controlled with a precision of ±0.05 log units. The temperature and location of the Deltech's hotspot was evaluated with a type-S thermocouple. All experiments

were performed using the Pt wire loop method. Powdered starting materials were mixed with a 3% polyvinyl alcohol solution to form a thick paste and loaded onto the wire loop. The polyvinyl alcohol solution served as an adhesive, binding the starting powder to the wire loop before it was loaded into the furnace.

The experimental charges were initially held at 1440˚C for at least one hour before cooling to a final temperature of 1300˚C. The cooling rates of the experiments was varied from 1.9˚C min^{-1} to 0.5˚C min^{-1}. Each charge was soaked for a minimum of 18 hours at the final dwell temperature before drop quenching into a beaker of water. Based on published experimental phase equilibria data, we estimate that the atmospheric pressure liquidus for our bulk composition falls in the range of 1430˚C-1450˚C (Presnall et al. 1978). The ternary phase diagram shown in Figure 1 shows both the phase relations for our experimental system, as well as the location of the starting bulk composition of our olivine growth experiments.

The oxygen fugacity of the olivine growth experiments was varied from ΔIW+1 to ΔIW-1.5. A total of four olivine growth experiments were performed as a part of this study. Only one of these experiments, ADF#4, contained enough olivine phenocrysts of sufficient size for the acquisition of multiple XANES spectra. Experiment ADF#4 was conducted with a cooling rate of 1.65 ˚C min^{-1} and an oxygen fugacity value of ΔIW-1.5.

Electron Microprobe Analysis

The experimental run products were mounted in thin epoxy wafers and polished for electron imaging and quantitative electron microprobe (EMP) analysis. EMP analyses were conducted using the JEOL JXA 8200 electron microprobe in the Institute of Meteoritics (IOM) at the University of New Mexico. Quantitative analyses were collected at an accelerating voltage of 15 kV, a current of 10 nA, and a 1 µm beam spot size. Standards consisted of a set of CM Taylor electron microprobe mineral standards. All data were reduced with a ZAF matrix correction algorithm native to the JEOL software. The compositional data obtained for the olivine and glass from experiment ADF#4 is presented in Table 1.

Electron Back Scatter Diffraction Analysis

Crystallographic orientations of selected olivine phenocrysts in experiment ADF#4 were determined by electron backscatter diffraction (EBSD) analysis. To ensure that a wide range of olivine orientations were sampled in the course of the EBSD analysis, specific crystals of interest were pre-selected. These crystals were chosen based on their apparent orientations as inferred from their shape, symmetry, and interfacial angles (Welsch et al. 2010).

The EBSD analyses of the olivine were collected with a JEOL 6700F field emission scanning electron microscope at the University of Nevada, Las Vegas, using an Oxford Instrument HKL system and Channel 5 software. The epoxy mounted sample was sectioned to suitable size and polished with a 0.05 µm colloidal silica suspension on a VibroMet vibratory polisher. The electron microscope was set to 20 KeV with 20 nA beam current. The sample was mounted on a 70˚ pre-tilted holder and faced horizontally to the detector at a working distance of 23 mm. Forsterite was selected as the Match Unit in Flamenco Acquisition software, with number of reflectors 60 and HoughRes 60. The scanned area of the olivine crystals was typically greater than 2/3 of the total exposed area. The EBSD patterns were collected automatically at 0.5 mm step intervals. The orientations were determined using Channel 5 Mambo software. With this software, each of indexed EBSD patterns from a given area scan were collectively converted into an upper hemisphere pole figure (i.e., a stereographic projection) that shows the orientation of the a, b, and c crystallographic axes for the olivine crystal of interest. The densities of calculated orientations have been color coded in the pole figures; in this scheme the warm colors represent the highest density of orientation data points whereas the cool colors represent the lowest density of data points.

XANES Spectra Acquisition and Data Reduction

Chromium K-edge XANES data were acquired with the x-ray microprobe of beamline 13-ID-E at the Advanced Photon Source (APS), Argonne National Laboratory, Illinois. The x-ray source at APS beamline 13-ID-E was a 62-pole, 36 mm period undulator. The linearly polarized beam was focused to final spot size of approximately 2µm by 2µm with dynamically configured Kirkpatrick-Baez focusing mirrors. All spectra were acquired in fluorescence mode utilizing a cryogenically cooled Si (111) monochromater coupled with a silicon-drift x-ray detector offset

178 at a 45° angle from the sample. The monochromater energy was calibrated using metallic Cr
179 foil.

180 The Cr K-edge spectra were collected over the energy range of 5993 eV to 6289 eV. The
181 monochromater energy step width was set to 0.1 eV in the energy range of 5984 eV to 6009 eV
182 and was increased to 5.0 eV in the regions of the spectrum outside of the 0.1 eV energy step
183 window. The distance between the sample surface and the silicon-drift detector was optimized
184 to maximize the x-ray count rates while minimizing the detector dead time. A minimum of
185 three spectra were acquired in each olivine phenocryst, always confined to the center of the
186 crystal, typically within a 10 μm radius of one another. These groups of spectra were obtained
187 for olivine in different orientations (relative to the beam polarization) by rotating the sample in
188 increments of 45˚ after the completion of each measurement.

189 All spectra were processed using the Athena software package (Ravel and Newville 2005).
190 Processing began by normalizing the x-ray count rate to the incident beam flux that was
191 measured with an ion chamber upstream of the focusing mirrors. The spectra were then
192 smoothed with five iterations of a three-point averaging algorithm and post-edge normalized.
193 The extraction of Cr valence ratios from the spectra followed the procedures outlined in Berry
194 et al. (2006), Goodrich et al. (2013) and Bell et al. (2014). This data reduction scheme relies on
195 the intensity absorption that is associated with the 1s-4s electron transition. Although formally
196 dipole forbidden, this electron transition is allowed for Cr^{2+} in Jahn-Teller distorted octahedral
197 coordination in olivine. The Jahn Teller distorted coordination symmetry enhances orbital
198 mixing, thus loosening the formal restrictions of Laporte's selection rule and increasing
199 intensity absorption associated with the 1s-4s transition. The link between presence of Cr^{2+} and
200 the presence of the 1s-4s absorption peaks is the foundation for XANES-based Cr valence
201 measurements, as the intensity of this feature is linearly proportional to the $Cr^{2+}/\Sigma Cr$ of the
202 material being analyzed (Berry et al 2004, and Berry and O'Neill. 2006). As previous studies
203 have shown, the intensity of the 1s-4s absorption features is best quantified using the first
204 derivative of the normalized spectra, where this peak is centered at approximately 5994 eV.

205 The intensity of the 1s-4s absorption was measured for each of the olivine spectra, as well
206 as spectra obtained for the equilibrium liquid. The measured 1s-4s absorption intensities (or

207 "peak heights") were converted into $Cr^{2+}/\Sigma Cr$ values for the olivine crystals and glasses via a
208 linear interpolation anchored by the measured 1s-4s absorption intensities of Cr^{2+} and Cr^{3+}
209 reference materials. The Cr^{2+} and Cr^{3+} standards used in the data reduction scheme consisted of
210 two glasses that were produced in the study of Hanson and Jones (1998). The canonical
211 absorption intensity values for these standards used in our data reduction scheme were 0.215
212 and 0.01 for the Cr^{2+} ($Cr^{2+}/\Sigma Cr$ =0.95) and Cr^{3+} ($Cr^{2+}/\Sigma Cr$ =0.01) glass standards, respectively.
213 The Hanson and Jones (1998) glass standards were chosen out of necessity, as no end-
214 member olivines with independently characterized Cr valence are currently available for use as
215 reference materials. The use of glasses as standards is predicated on the assumption
216 coordination geometry of Cr^{3+} and Cr^{2+} in the olivine structure and the quenched glass are
217 equivalent. The evidence and observations supporting this assumption is discussed in following
218 paragraphs.
219 Crystal field theory predicts that Cr^{3+} has a strong octahedral site preference in silicate
220 materials, likely precluding the presence of lower symmetry coordination states in either
221 silicate glasses or olivine (Burns 1974). Several spectroscopic studies also lend additional,
222 concrete support to the crystal field theory predictions. For example, several spectroscopic
223 studies independently concluded that Cr^{3+} adopts regular octahedral coordination in quenched
224 silicate glasses (Keppler 1992 and Vallain et al. 2010). Additionally, there is some available
225 spectroscopic evidence suggesting that Cr^{3+} in olivine is also present in a regular octahedral
226 coordination geometry. An electron paramagnetic resonance spectroscopy study focusing on Cr
227 doped synthetic forsterite concluded that Cr^{3+} occupies the octahedral olivine M1 site, where
228 local charge balance is maintained by a vacancy present in an adjacent M1 site (Shakurov
229 & Tarasov 2001).
230 There are also several independent lines of evidence indicating that Cr^{2+} is present in a
231 highly distorted octahedral coordination state in both silicate melts and the olivine structure. It
232 is well known that divalent Cr is a Jahn-Teller active cation (Burns 1974), therefore causing it to
233 adopt a lower symmetry, axially-distorted, octahedral coordination geometry. A UV-VIS
234 spectroscopic study by Keppler (1992) of anorthite-diopside and albite glasses concluded that
235 Cr^{2+} occupies highly distorted octahedral sites in the glass structure. On the olivine side of the

coin, an EXAFS study of Cr bearing olivine by McKeown et al. (2014) showed that Cr^{2+} occupies the M1 site in a coordination geometry that in a tetragonally compressed hybrid of the regular M1 octahedral site and a square planar site.

In addition to the evidence from the studies cited in preceding discussion, it should also be noted that the suitability of the Hanson and Jones glasses as standards for calculating Cr valence ratios in olivine was evaluated in the study of Goodrich et al. (2013). That work demonstrated that the use of these glasses as standard reference materials did in fact yield accurate Cr valence values for a powdered, synthetic, Cr^{2+}-dominated forsterite sample with an independently known $Cr^{2+}/\Sigma Cr$ value.

We have also attempted to assess the reproducibility of the Cr^{2+}peak intensity at 5994 eV. To accomplish this, we have performed a set of seven replicate XANES analyses on a Cr-doped, low liquidus CMAS quenched glass. The composition of this melt was patterned after a low liquidus composition investigated by Longhi (1987). This CMAS liquid was equilibrated for 23 hours at a $\log_{10}fO_2$ value of -9.60 and a temperature of 1400˚C in the gas mixing laboratory at UNM. The measured 1s-4s peak intensities from replicate analyses on this glass yielded a mean absorption intensity of 0.1425 with a 1σ standard deviation of ±0.0025. From these analyses, we estimate that the intrinsic uncertainty associated with the peak intensity measurements is ± 1.8 %, relative.

Determining the Crystallographic Orientation of Experimental Olivine

Constructing a model that quantitatively describes the XANES anisotropy observed for olivine requires that the polarization direction of the beam be known relative to the orientation of the olivine crystallographic axes. In the spherical coordinate system, two angles (ϕ and θ) can be used to uniquely define the beam's polarization direction relative to the olivine's orientation. Figure 2 shows how these angles are defined with respect to the reference frame of the olivine's a, b, and c axes. The values of ϕ and θ associated with each XANES spectral acquisition were calculated using the Stereonet 9 software package (Cardozo et al., 2013). The a, b, and c crystallographic axis were plotted on a stereonet, along with the polarization vector for the beam. The value of θ is defined as the angle between polarization vector projected onto

the a-b plane and the a-axis, and the value of ϕ is defined as the angle between the c-axis and the polarization vector.

The orientation of an olivine's crystallographic axes as it was determined during the EBSD analysis was rarely coincident with its orientation during the XANES spectra acquisition. Therefore, the calculation of the ϕ and θ angles required a transformation of the stereographic projection of olivine's axes in the EBSD orientation to orientation in which the XANES spectra was acquired. Put simply, the EBSD orientations were restored to match the orientation of the crystal during the XANES analyses by rotating the projection of the olivine's axes about an axis normal to the sample surface (i.e. the pole represented by the center-point of the stereographic projection). The magnitude of the rotation of the required for this correction was determined by comparing reflected images of the olivine taken during each of the three sequential XANES analyses, each separated by 45 degrees, to the back scattered electron images collected during the EBSD analyses.

RESULTS AND DISCUSSION

Experiments

All of the XANES and EBSD data presented here were obtained from olivine crystals and equilibrium liquid in experiment ADF#4. This experiment contained a phase assemblage consisting of olivine and quenched melt. Based on a visual estimation, this experiment contained approximately 15-20% euhedral olivine crystals. With the exception of a few elongate, blade-like crystals that were confined to the center of the experimental charge, the morphology of the olivine crystals can be described as equant euhedral to tabular euhedral. The size of these phenocrysts ranged from approximately 50 µm to 150 µm along their maximum dimension. Figure 3 shows an annotated backscattered electron image of the stable phase assemblage present in ADF#4. This BSE image also indicates which olivine crystals were used in the combined XANES/EBSD analyses.

The olivine crystals in ADF#4 were essentially end-member forsterite (Fo_{100}), containing less than 1.0 wt. % of other components such as FeO, Cr_2O_3, and CaO. The mean EMP measured Cr_2O_3 concentration for ADF#4 olivines was 0.36 wt. % with a 1σ standard deviation of ± 0.02;

294 the Cr_2O_3 concentration of the quenched liquid was 0.51 ± 0.03. The complete chemistry of the
295 quenched melt and olivine from ADF#4, as determined by EMP, are provided in Table 1.
296 Using the EMP measurements, we calculated a Cr^{total} mineral-melt partition coefficient
297 value of 0.71, with a propagated 1σ uncertainty of ± 0.065. Our calculated DCr^{total} is in good
298 agreement with the DCr^{total} values determined by Hanson and Jones (1998). At 1320˚C, the
299 DCr^{total} values from the Hanson and Jones (1998) FAD1 experiments -the bulk composition of
300 which is a resonably good approximation for the bulk composition of our olivine growth
301 experiments, are 0.71 and 0.75 for fO_2 values of ΔIW+0 and ΔIW-3.5, respectively.
302 It is also worth noting that the color of the quenched experimental glass in ADF#4 was a
303 deep sapphire blue, consistent with the observations of previous studies (Keppler 1992). The
304 color of Fe-free, Cr-doped glasses has been noted as it is a sensitive, albeit qualitative, indicator
305 of the dominant Cr valence state of the glass, where the color blue is typically associated with
306 glasses dominated by Cr^{2+} whereas green is typically associated with those dominated by Cr^{3+}
307 (Keppler 1992).
308 As mentioned earlier, the experimental suite included additional samples not addressed in
309 this manuscript. Those samples were crystallized at higher fO_2 values (IW+1) and contained Cr-
310 rich spinel in addition to euhedral olivine and quenched glass. Those spinels often occurred as
311 inclusions within the phenocrystic olivine, therefore we concluded that their presence may
312 compromise the XANES spectra from the olivine, and were therefore excluded from further
313 XANES analyses.
314
315 **EBSD Analysis & Olivine Orientations**
316 Figure 4 shows an example of the EBSD-determined orientation for one of the
317 experimentally grown olivine crystals (Oliv#4). Using the pole figures derived from the EBSD
318 analysis of the olivines, the XANES orientations of the olivines were determined following the
319 procedure outlined in the methods section; the orientations are given as the angles ϕ and θ in
320 Table 2. The pole figures from all of the olivine phenocrysts listed in Table 2 are included in
321 Electronic Appendix 1.
322
323 **XANES Results for Olivine and Quenched Melt**

The XANES analyses for the chosen population of olivine crystals in ADF#4 yielded a broad range of values with respect the intensities of the Cr^{2+} absorption feature. Measured intensities for the Cr^{2+} absorption feature range from a minimum value of 0.179 to a maximum value of 0.258. Table 2 provides the absorption intensities for each olivine measured, as well as its corresponding orientation relative to the beam polarization (given as angles ϕ and θ). Given that the $Cr^{2+}/\Sigma Cr$ values of the olivines are ostensibly identical, as the entire population was grown in a single equilibrium crystallization experiment, the observed variation is a direct manifestation of the effects of the absorption anisotropy.

Figure 6 illustrates the effect of crystallographic orientation on the intensity of the 1s-4s absorption for a single olivine crystal. The plot in Figure 6 shows the derivative spectra of a single experimental olivine crystal (Oliv#4) in three distinct orientations. These spectra show how the magnitude of the 1s-4s absorption intensity varies for this crystal as a function the angles ϕ and θ. The a-axis of Oliv#4 is approximately normal to the polished sample surface, or stated differently, the polished sample surface is roughly coincident with a plane containing the the b and c axes. Simply rotating the orientation of the b-c plane by 90˚ (from orientation #1 to orientation #3) results in a 24% reduction in the observed 1s-4s absorption intensity. Not surprisingly, the absorption intensities of the entire population of olivine analyses also show significant dispersion. The difference between the highest and lowest observed absorption intensities is ~30%. This variation is at least an order of magnitude greater than the analytical uncertainty of the measurements, and places a minimum constraint on the extent to which absorption anisotropy should affect CrViO measurements.

To illustrate how the anisotropy can distort the results of Cr valence measurements, we have converted measured intensities of our olivine population into “apparent” Cr valence values. In this instance, we use the term “apparent” to describe the Cr valence value that is distorted by anisotropy absorption. The resulting values are listed in Table 2 and shown graphically in Figure 6. The olivine Cr valence values illustrate that two important effects precipitated by the XANES anisotropy. The first is that the anisotropic absorption causes a wide dispersion (~30%) with respect to the “apparent” valence values for the olivine. The observed absorption variability is a good match for the differences in absorption intensity that were

353 attributed to anisotropy in Goodrich et al. (2013). The authors of this study suggested that the
354 maximum anisotropic dispersion observed for their measured Cr valence values was
355 approximately ±16-19%, or rather a range of 36%.

356 A second, but equally important effect can be observed for spectra that show the highest
357 Cr^{2+} absorption intensities. The conversion of these intensities to Cr valence values yields
358 unrealistically low Cr valence values. In our olivine dataset, 25% of the apparent Cr valence
359 values (i.e., 5 of 20) indicate that these olivines have a mean Cr valence that is less than 2.0,
360 which suggests that they contain a significant fraction of monovalent Cr. If valence data from
361 these spectra were alternatively cast as $Cr^{2+}/\Sigma Cr$, the values are >1.0, further confusing the
362 matter. The calculated Cr valence values for these olivines are clearly a specious artifact of the
363 effects of absorption anisotropy, as monovalent Cr has never been observed in either minerals
364 or glasses. Furthermore, the fact that the liquid from which the experimental olivines grew
365 contained a binary mixture of Cr^{2+} and Cr^{3+} ($Cr^{2+}/\Sigma Cr = 0.76$) also suggests that the low apparent
366 valence values should not be interpreted literally.

367 Artificially low Cr valence values can also be observed for a single olivine crystal. For
368 example, the Cr valence values for Oliv#4 (see Figure 4) range from a spurious low of value 1.98
369 to a high of 2.22. Variations in the apparent Cr valence values for Oliv#4 are correlated with the
370 values of θ and ϕ, and for one of the orientations the intensity of the Cr^{2+} absorption feature
371 even exceeds that of the Cr^{2+} standard. From this observation we conclude that for olivine
372 crystals rich in Cr^{2+}, there exists a range of orientations for which the 1s-4s peak height is
373 greater than that of an isotropic Cr^{2+} standard material. Reiterating the point made above, the
374 low Cr values are simply an artifact of the data reduction, however that is not to say that the
375 isotropic standard is inappropriate for the crystalline olivine samples, but rather, the individual
376 spectra from single crystals of anisotropic materials need to be distilled to their "isotropic"
377 values to place them on equal footing with the standards. Alternatively, the problem could also
378 be mitigated with the use of a standard olivine spectrum that was acquired in an identical
379 orientation to that of the crystal being analyzed. Although artificially low Cr valences are clearly
380 an issue for the reduced, low Cr^{3+} olivine crystals used in this study, it should be stressed that
381 that this effect is likely restricted to olivine that is highly enriched in Cr^{2+} (>85%), as 1s-4s

absorption intensities for olivines with lower $Cr^{2+}/\Sigma Cr$ should not exceed those of the standard reference material.

Modeling the XANES Anisotropy as a Function of Crystallographic Orientation

The XANES results for the olivine discussed in the previous section demonstrate the outstanding need for the development of an orientation correction. In order to develop an orientation correction scheme, it is first necessary to model the absorption anisotropy as a function of the angles that define the olivine's orientation, θ and ϕ. To accomplish this, we have chosen to model the angular dependence of the intensity of the absorption peak associational with Cr^{2+} with an ellipsoidal function, where the measured Cr^{2+} absorption intensity is represented by radius of the ellipsoid for specified values of θ and ϕ. In spherical coordinates the angular dependence of the absorption ellipsoid is given by:

Eq.1
$$A_{(\theta,\varphi)} = \left[\frac{\cos^2\theta \sin^2\phi}{a^2} + \frac{\sin^2\theta \sin^2\phi}{b^2} + \frac{\cos^2\phi}{c^2}\right]^{-0.5}$$

Where a, b, and c are the lengths of the principle three axes describing the ellipsoid; these values are also the absorption intensities if the electric field direction of the beam was coincident with the direction of the indicatrix axis. In our modeling we assume that the three principle axes of the x-ray indicatrix are the same as the olivine's a, b, and c crystallographic axes, or in other words the axes of the indicatrix ellipsoid are coincident with the olivine's crystallographic axes. This assumption is well justified by the results of a study by Dyar et al. (2002b), in which the authors concluded the x-ray absorption indicatrix is analogous to the optical indicatrix for minerals, in that the crystal system of the mineral dictates how the three principle indicatrix axes are related to the crystallographic axes. For olivine, this means that the orientation of the indicatrix axes (i.e. a, b, & c in Eq.1) and is aligned with that of crystallographic axes.

Here we should stress that the major objective of the study was to develop an empirical anisotropy correction, therefore, we have concentrated our efforts on producing model that accurately predicts the variation in absorption intensity. Ideally the absorption ellipsoid for

411 olivine would be defined by obtaining spectra in orientations where the polarization vector of
412 the beam is coincident with each of the crystallographic axes (i.e. the end-member
413 orientations); however, this is not practical for natural olivine in thin sections or the small
414 experimental olivine in our experiments. The EBSD we employ in this study method presents a
415 way to circumvent this issue. The absorption intensities for the end-member orientations can
416 be predicted from the absorption ellipsoid fit to the calibration dataset, provided a sufficient
417 range of φ and θ angles are sampled.

418 We have fit the absorption oriented olivine data to Eq.1 via least squares minimization using
419 a non-linear GRG algorithm. This fitting yielded the following values for the ellipsoid axes:
420 a=0.1882, b=0.2592 and c= 0.1692. Figure 7 shows a plot of the measured intensity values vs.
421 the predicted values; the various colors of the data points are used to denote the olivine crystal
422 from which each data point originated. To assess the goodness of the fit we have calculated
423 the reduced χ^2 statistic for the model. Using the estimated error of value ±1.9% for the
424 measured peak intensities we calculate a $\chi^2 = 22.62$ (17 degrees of freedom with a critical value
425 of 27.58 at the 95% confidence level) and a reduced χ^2 value of 1.33 (i.e. χ^2/d.o.f.); the
426 calculated χ^2 values suggest the ellipsoidal model is statistically robust fit for the oriented
427 olivine absorption dataset. The reduced χ^2 value indicates that the ellipsoidal model is a
428 statistically good description for the angular dependence of the 1s-4s absorption features in our
429 dataset. The absorption ellipsoid produced with our dataset predicts that the measured
430 intensities should vary with a range (e.g. (max-min)/max) of ~34% relative. This value is in good
431 agreement with the effects of anisotropy observed in the Goodrich et al. (2013) study, where
432 the authors report a maximum range of 38%.

433 It should be pointed out that that the fitting of the absorption ellipsoid in of itself does not
434 constitute an anisotropy correction; rather, the ellipsoid is simply a quantitative description the
435 relationship between the absorption intensity and the crystallographic orientation of the
436 sample. The calibration of the absorption ellipsoid for olivine is an integral part of formulating
437 an anisotropy correction, as the relationship between the observed absorption intensity and
438 the "isotropic" absorption intensity (i.e. the mean absorption intensity that would be obtained
439 for a powder of randomly oriented crystals) are a function of angles θ and ϕ. In other words,

given values of θ and ϕ the absorption ellipsoid can be used calculate a correction coefficient. The anisotropy correction coefficient (abbreviated as ACC) can then be used restore any measured 1s-4s intensity from a spectrum obtained at known θ and ϕ to its isotropic value. The ACC is defined as the ratio of the isotropic absorption intensity to the observed absorption intensity for a particular orientation:

Eq. 2 $$\frac{A_{(i)}}{A_{(\theta,\varphi)}} = ACC$$

Where $A_{(i)}$ is the isotropic absorption intensity (i.e., the value that yields the correct bulk $Cr^{2+}/\Sigma Cr$ for the olivine) and $A_{(\theta,\phi)}$ is the absorption intensity measured at θ and ϕ. Practically speaking, the $A_{(i)}$ is simply the reference point to which the absorption data are should be restored. Substituting Eq. 1 into Eq. 2 yields the equation for the ACC:

Eq.3 $$ACC = \left(\left[\frac{\cos^2\theta \sin^2\phi}{a^2} + \frac{\sin^2\theta \sin^2\phi}{b^2} + \frac{\cos^2\phi}{c^2}\right]^{0.5}\right) A_{(i)}$$

In order for Eq. 3 to be of practical use for correcting CrVIO measurements the values of a, b, c, and $A_{(i)}$ must be known for the calibration olivine. As it was impractical to retrieve the value of $A_{(i)}$ using spectra measured for powdered olivine from ADF#4, we have opted to determine this value by calculating the geometric mean of the absorption ellipsoid axes. In this approach, using the geometric mean of a, b, and c is equivalent converting the absorption ellipsoid to a sphere of equal volume and using the radius of this sphere as the isotropic absorption value for our dataset. In other words, converting the ellipsoid into sphere of equal volume via the geometric mean is a simple way of approximating the "mean" or isotropic absorption intensity for the olivine in our dataset. With this approach we calculate an $A_{(i)}$ value of 0.2021, which yields a $Cr^{2+}/\Sigma Cr$ of 0.89 for the ADF#4 olivine. In contrast, simply using the mean of the measured intensities from the entire dataset of the ADF#4 olivine crystals yields $Cr^{2+}/\Sigma Cr$= 0.92 and an $A_{(i)}$ of 0.2088; this value is likely not as accurate as the value derived from the geometric mean of

467 the axes, as it may be biased by the virtue of the fact that our intensity dataset over represents
468 olivine with θ and ϕ angles that correspond to high absorption intensities.

469 Correcting olivine Cr K-edge XANES with Eq. 3 substantially increases the accuracy of the
470 measured $Cr^{2+}/\Sigma Cr$ values. To illustrate this point, we will use the XANES results from Ol#4.
471 Depending on the orientation in which the XANES spectrum was obtained, the $Cr^{2+}/\Sigma Cr$ values
472 calculated for this olivine are 0.77, 0.91, and 1.0. Without the application of an orientation
473 correction, it is obviously difficult to discern which, if any, of the measured values accurately
474 reflects the actual $Cr^{2+}/\Sigma Cr$ of the crystal. It should be stressed that although the intrinsic
475 uncertainty for a measurement made on a phenocryst in a single orientation may be low (e.g.
476 ±1.8%), the error with respect to the accuracy of the value will likely be substantially higher
477 than 1.8%, given a totally random orientation. We conservatively estimate that the application
478 of the ACC reduces the orientation induced uncertainty in the measured intensity of the Cr^{2+}
479 absorption feature to ± 0.50, which translates to a $Cr^{2+}/\Sigma Cr$ error of ± 0.03. This is a substantial
480 improvement in the accuracy of XANES measured $Cr^{2+}/\Sigma Cr$ values in olivine where the
481 orientation related uncertainty has been reduced from ± 0.17 to ± 0.03, or roughly a factor of
482 five.
483

484 **IMPLICATIONS**

485 To illustrate the importance of the orientation correction for obtaining accurate fO_2 values,
486 will use the following hypothetical example. Consider the olivine phenocrysts crystallized from
487 a hypothetical basaltic liquid at 1200°C with an fO_2 value of ΔFMQ-1 ($\log_{10}fO_2$= -8.3) and a
488 $Cr^{2+}/\sum Cr$ of 0.50. (i.e., these conditions correspond to lnK'= 4.77 for the homogenous CrO-
489 $CrO_{1.5}$ equilibrium). The olivine that crystallizes from this melt should have a $Cr^{2+}/\sum Cr$ value
490 identical to that of its parental liquid, as the values $D_{ol\text{-}liq}Cr^{2+}$ and $D_{ol\text{-}liq}Cr^{3+}$ are numerically
491 indistinguishable in basaltic magmas (Gaetani and Grove 1997, Canil 2001, and Mallmann and
492 O'Neill 2009). If an olivine phenocryst in a random, unknown crystallographic orientation were
493 chosen for XANES analysis its apparent $Cr^{2+}/\sum Cr$ could assume any value ranging from
494 approximately 0.65 to 0.35. Converting the $Cr^{2+}/\sum Cr$ values into numerical oxygen fugacity
495 values with the equations outlined in Berry et al. (2006) and expanded upon in Bell et al. (2014),

yields a $\log_{10}fO_2$ of -9.4 for $Cr^{2+}/\sum Cr = 0.65$ and a $\log_{10}fO_2$ of -7.2 for $Cr^{2+}/\sum Cr = 0.35$, or a range of ΔFMQ-2.1 to ΔFMQ+0.1.

It is also worth noting that one of the more attractive aspects of the proposed CrViO oxybarometer is that it can perhaps provide a continuous record of fO_2 for the entire olivine crystallization interval. The ability of olivine to potentially capture dynamic variations in magmatic fO_2 renders it an especially useful tool for understanding how processes such as volatile exsolution, auto-oxidation, or crustal assimilation control magmatic fO_2 values in basaltic magmas. It should also be reiterated that the CrViO can potentially be applied to olivine-bearing magmatic rocks that do not contain quenched melts or glassy melt inclusions. This point is of considerable importance as the use of $Fe^{3+}/\sum Fe$ measurements to calculate magmatic fO_2 values is currently limited to magmatic rocks that contain a glassy phase.

Although a significant amount of development still needs to be completed before the CrViO oxybarometer becomes a fully functional tool, the anisotropy correction developed in this this work represents a vital step in that direction.

Acknowledgements

This work was funded by NSF EAR 1550929 awarded to ASB. Portions of this work were performed at GeoSoilEnviroCARS (The University of Chicago, Sector 13), Advanced PhotonSource (APS), Argonne National Laboratory. GeoSoilEnviroCARS is supported by the National Science Foundation - Earth Sciences (EAR-1128799) and Department of Energy-GeoSciences (DE-FG02-94ER14466). This research used resources of the Advanced Photon Source, a U.S. Department of Energy (DOE) Office of Science User Facility operated for the DOE Office of Science by Argonne National Laboratory under Contract No. DE-AC02-06CH11357. M.D. Dyar and M. Jercinovic are both thanked for their thoughtful reviews of the manuscript. These reviews substantially improved version of the paper.

REFERENCES

Bell, A.S., Burger, P.V., Le, L., Shearer, C.K., Papike, J.J., Sutton, S.R., Newville, M., and Jones, J. (2014) XANES measurements of Cr valence in olivine and their applications to planetary basalts. American Mineralogist, 99, 1404–1412.

Berry, A.J., and O'Neill, H.St.C. (2004) A XANES determination of the oxidation state of chromium in silicate glasses. American Mineralogist, 89, 790-798.

Berry, A.J., O'Neill, H.St.C., Scott, D.R., Foran, G.J., and Shelley, J.M.G. (2006) The effect of composition on Cr2+/Cr3+ in silicate melts. American Mineralogist, 91, 1901–1908.

Cardozo, N., and Allmendinger, R.W. (2013) Spherical projections with OSXStereonet, Computers & Geosciences, 51, 193-205

Dyar, M.D., Gunter, M.E., Delaney, J.S., Lanzarotti, A., and Sutton, S.R. (2002a) Systematics in the structure and XANES spectra of pyroxenes, amphiboles, and micas as derived from oriented single crystals. Canadian Mineralogist, 40, 1375-1393.

Dyar, M.D., Gunter, M.E., Delaney, J.S., Lanzarotti, A., and Sutton, S.R. (2002b) Use of the spindle stage for orientation of single crystals for microXAS: Isotropy and anisotropy in Fe-XANES spectra. American Mineralogist, 87, 1500-1504

K.A. Evans, D.M. Dyar, S.M. Reddy, A. Lanzirotti, D.T. Adams, N. Tailbly (2014) Variation in XANES in biotite as a function of orientation, crystal composition and metamorphic history American Mineralogist, 99, 443-457

Goodrich, C.A., Sutton, S.R., Wirick, S., and Jercinovic, M. (2013) Valences of Cr in ureilite olivine and implications for ureilite petrogenesis. Geochimica et Cosmochimica Acta, 122, 280-305.

Hanson, B., and Jones, J.H. (1998) The systematics of Cr3+ and Cr2+ partitioning between olivine and liquid in the presence of spinel. American Mineralogist, 83, 669-684.

Longhi, J., 1987. Liquidus equilibria and solid solution in the system CaAl2Si2O8–Mg2SiO4–CaSiO3–SiO2 at low pressure. Am. J. Sci. 287, 265-331.

Presnall D. C., Dixon S. A., Dixon J. R., O'Donnell T. H., Brenner N. L., Schrock R. L., Dycus D. W. (1978) Liquidus phase relations on the join diopside–forsterite–anorthite from 1 atm to 20 kbar; their bearing on the generation and crystallization of basaltic magma. Contributions to Mineralogy and Petrology, 66, 203-220.

Ravel, B., and Newville, M. (2005) ATHENA, ARTEMIS, HEPHAESTUS: data analysis for X-ray absorption spectroscopy using IFEFFIT, Journal of Synchrotron Radiation 12, 537-541

Welsch, B., Faure, F., Famin, V., Baronnet, A., and Bachèlery, P. (2013) Dendritic crystallization: A single process for all the textures of olivine in basalts? Journal of Petrology, 54, 539-574.

This is a preprint, the final version is subject to change, of the American Mineralogist (MSA)
Cite as Authors (Year) Title. American Mineralogist, in press.
(DOI will not work until issue is live.) DOI: http://dx.doi.org/10.2138/am-2017-5911

Figure 1

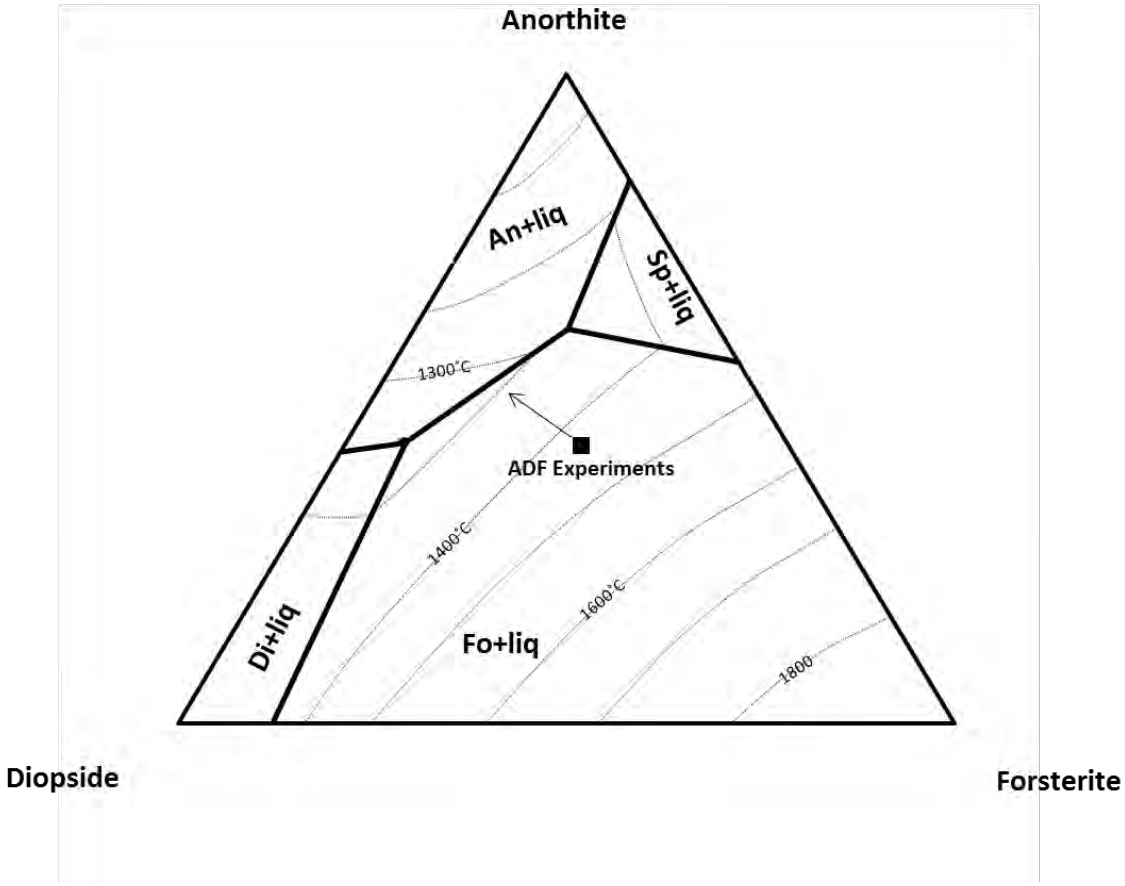

Figure 1 is a ternary plot that shows the starting bulk composition of the olivine growth experiments with respect to the phase relations in the An-Di-Fo system (after Presnall et al. 1978). The arrow represents the trajectory of the experimenal liquid as it was cooled below the olivine liquidus.

This is a preprint, the final version is subject to change, of the American Mineralogist (MSA)
Cite as Authors (Year) Title. American Mineralogist, in press.
(DOI will not work until issue is live.) DOI: http://dx.doi.org/10.2138/am-2017-5911

Figure 2

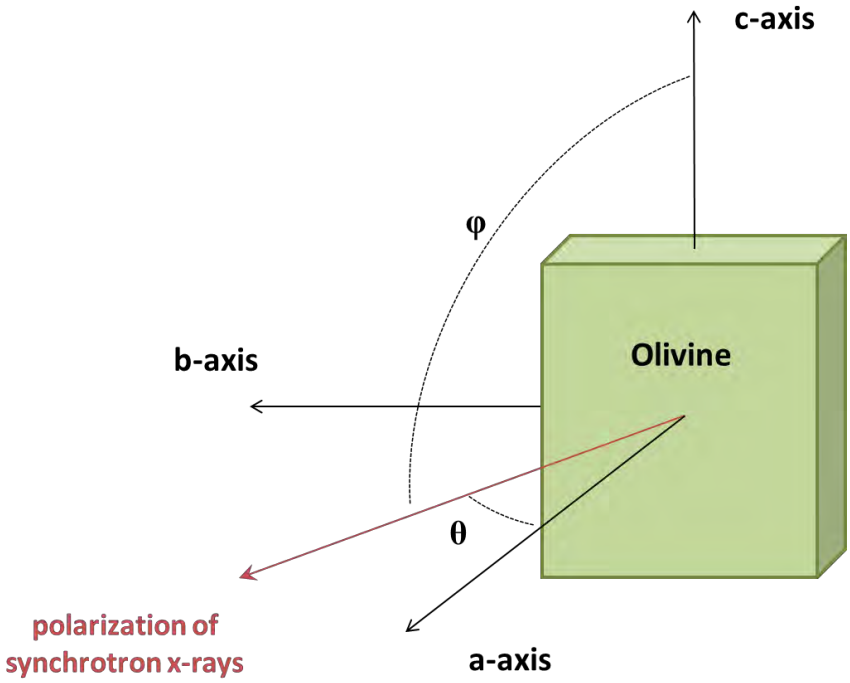

Figure 2 illustrates how the crystallographic axes of the olivine are related to the polarization direction of the synchrotron x-ray beam via the angles θ and ϕ. The EBSD determined orientations were used to calculate the angles θ and ϕ associated with each XANES spectrum used in this study.

This is a preprint, the final version is subject to change, of the American Mineralogist (MSA)
Cite as Authors (Year) Title. American Mineralogist, in press.
(DOI will not work until issue is live.) DOI: http://dx.doi.org/10.2138/am-2017-5911

Figure 3

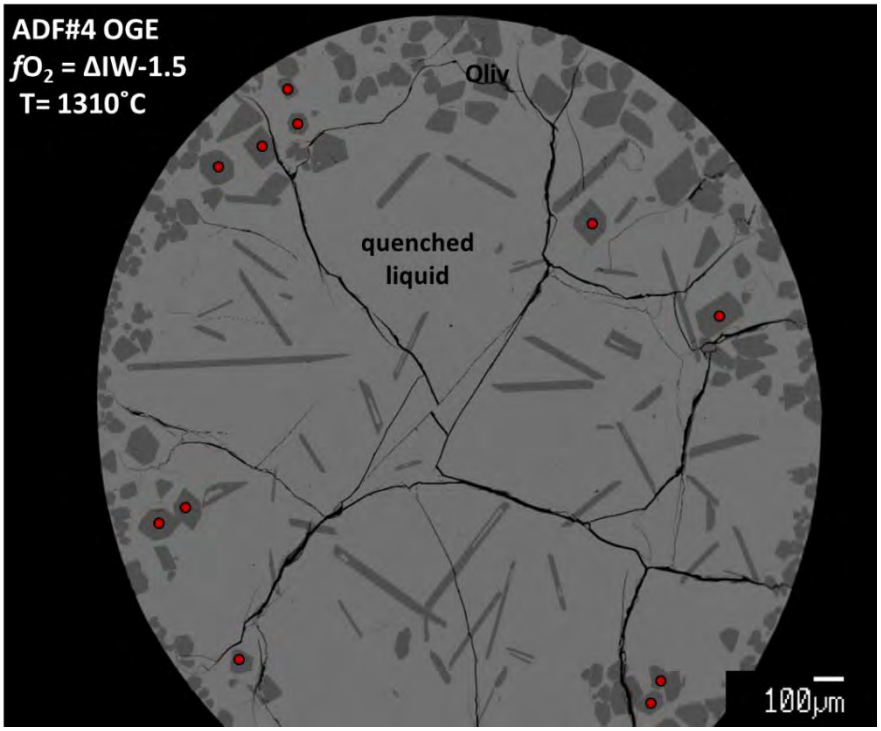

Figure 3 is a back scattered electron image (BSEI) of the experimental run products from ADF#4. The experiment shown in this BSEI contains only two phases - quenched melt and euhedral olivine crystals (Fo_{100}). The olivine crystals that were targeted for EBSD and XANES analysis have been denoted with a red spot.

This is a preprint, the final version is subject to change, of the American Mineralogist (MSA)
Cite as Authors (Year) Title. American Mineralogist, in press.
(DOI will not work until issue is live.) DOI: http://dx.doi.org/10.2138/am-2017-5911

Figure 4 a & b

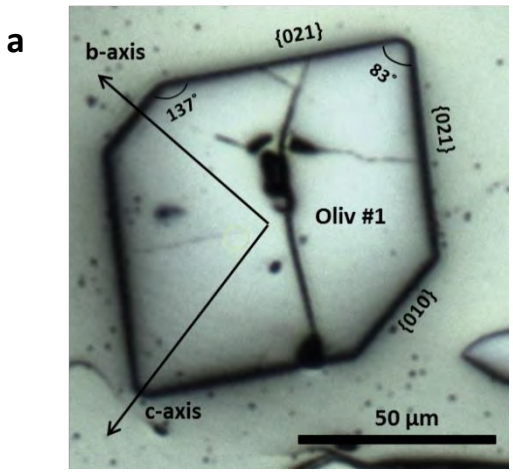

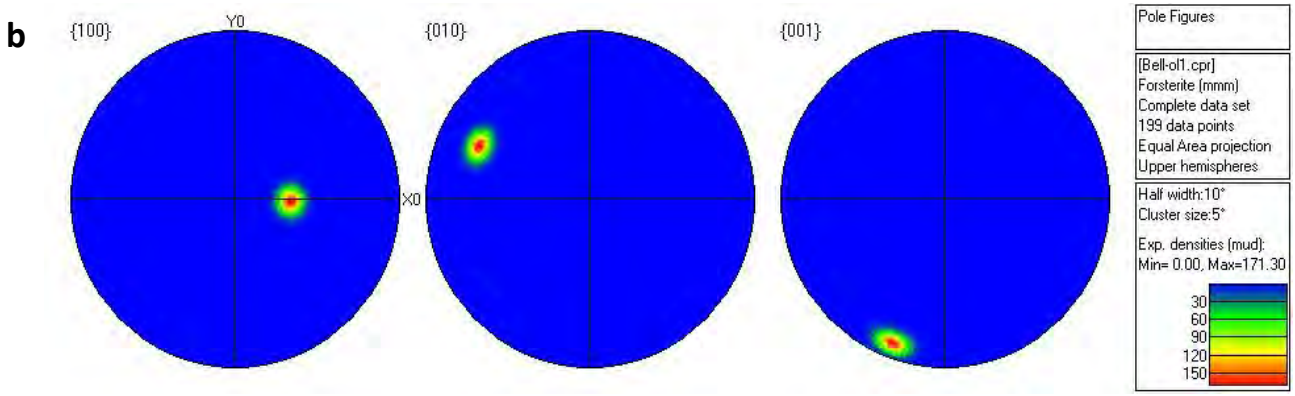

Figure 4a is a reflected light image of Ol#1 that has been annotated with the measured interfacial angles as well as miller indicies as they were inferred from the interfacial angles for several of the crystal faces; the inferred locations and orientations of the b and c axes are also annotated on the image (the a-axis comes out of the plane of the page) **4b** is an EBSD generated pole figure showing stereographic projections of the a, b, c, axes of the for Ol#1.

This is a preprint, the final version is subject to change, of the American Mineralogist (MSA)
Cite as Authors (Year) Title. American Mineralogist, in press.
(DOI will not work until issue is live.) DOI: http://dx.doi.org/10.2138/am-2017-5911

Figure 5

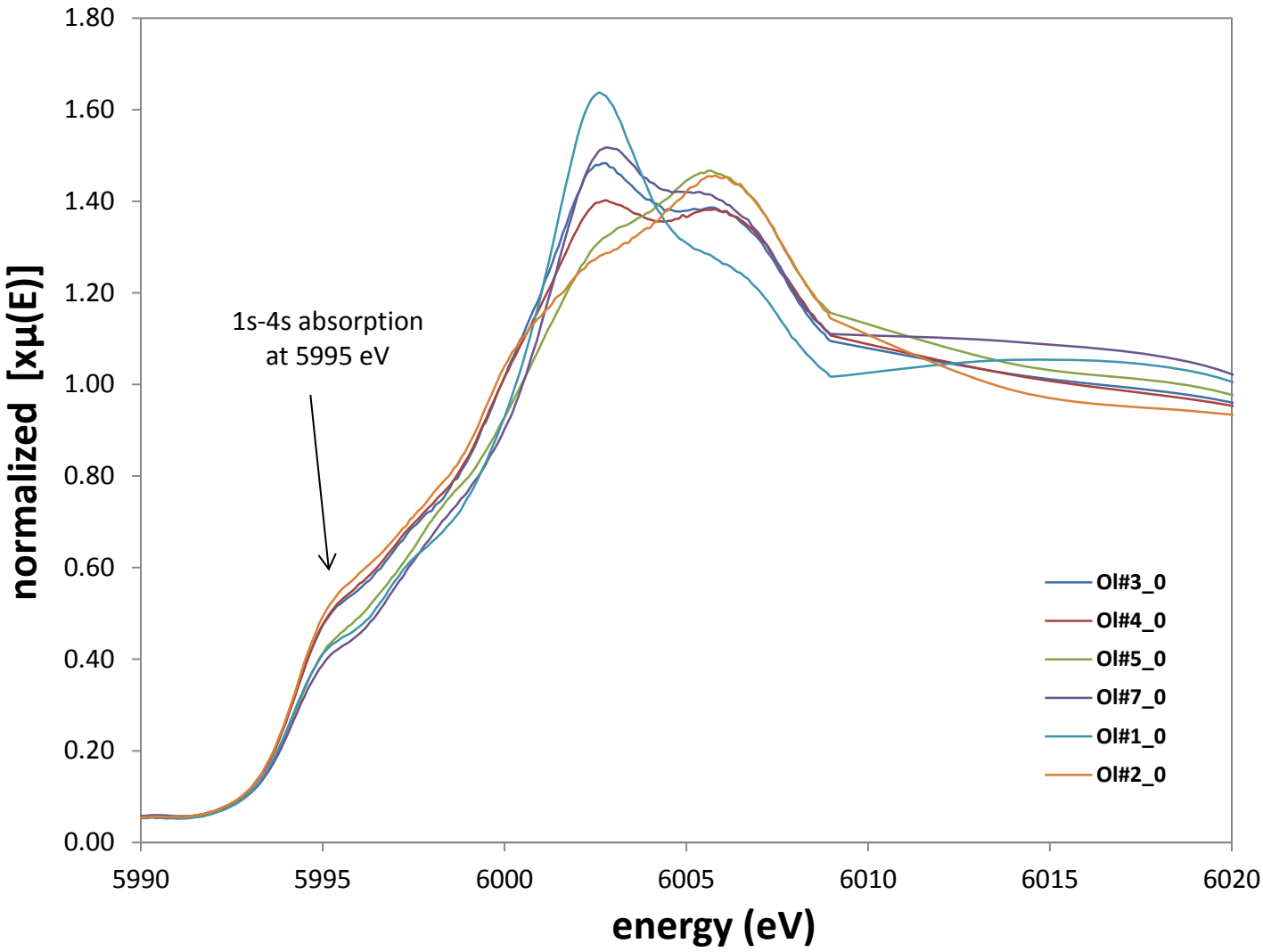

Figure 5 shows a set of normalized Cr K-edge spectra. Each of these spectra was taken from a different olivine crystal in the _0 orientation. These spectra clearly show that the intensities of the 1s-4s absoprtion features are affected by the orientation of the of the crystal during the spectra acqustition.

This is a preprint, the final version is subject to change, of the American Mineralogist (MSA)
Cite as Authors (Year) Title. American Mineralogist, in press.
(DOI will not work until issue is live.) DOI: http://dx.doi.org/10.2138/am-2017-5911

Figure 6

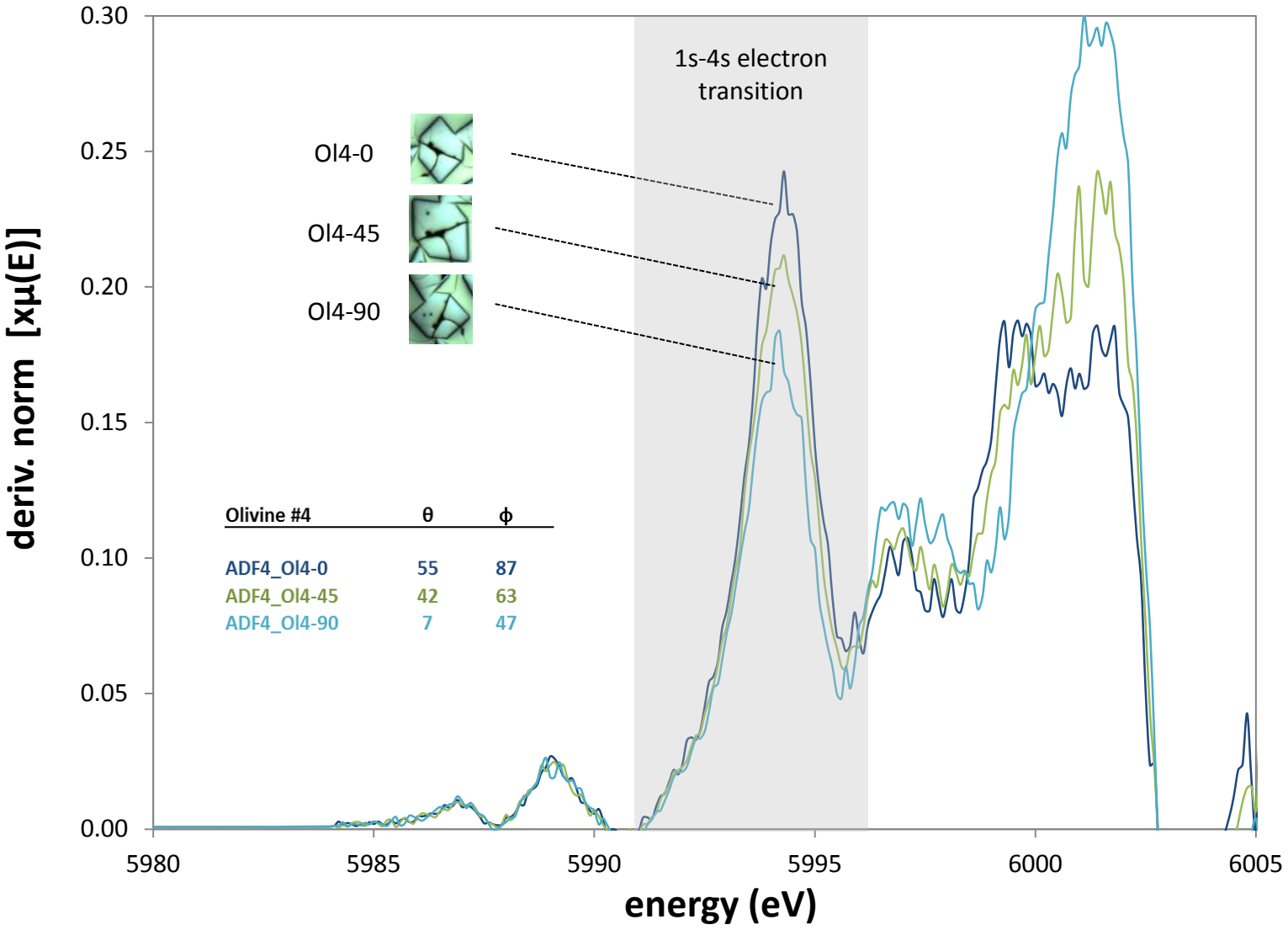

Figure 6 Illustrates the systematic variation in the intensity of the 1s-4s absorption as a function of the crystallographic orientation of an experimentally grown olivine crystal. Each spectra shown was obtained from the a single crystal (Ol#4) from OGE ADF#4. This crystal was rotated into three unique orientations relative to the beam polarization in order to obtain the three spectra shown. The intensity of the 1s-4s absorption varies nearly 25% as a function of changing orientation.

This is a preprint, the final version is subject to change, of the American Mineralogist (MSA)
Cite as Authors (Year) Title. American Mineralogist, in press.
(DOI will not work until issue is live.) DOI: http://dx.doi.org/10.2138/am-2017-5911

Figure 7

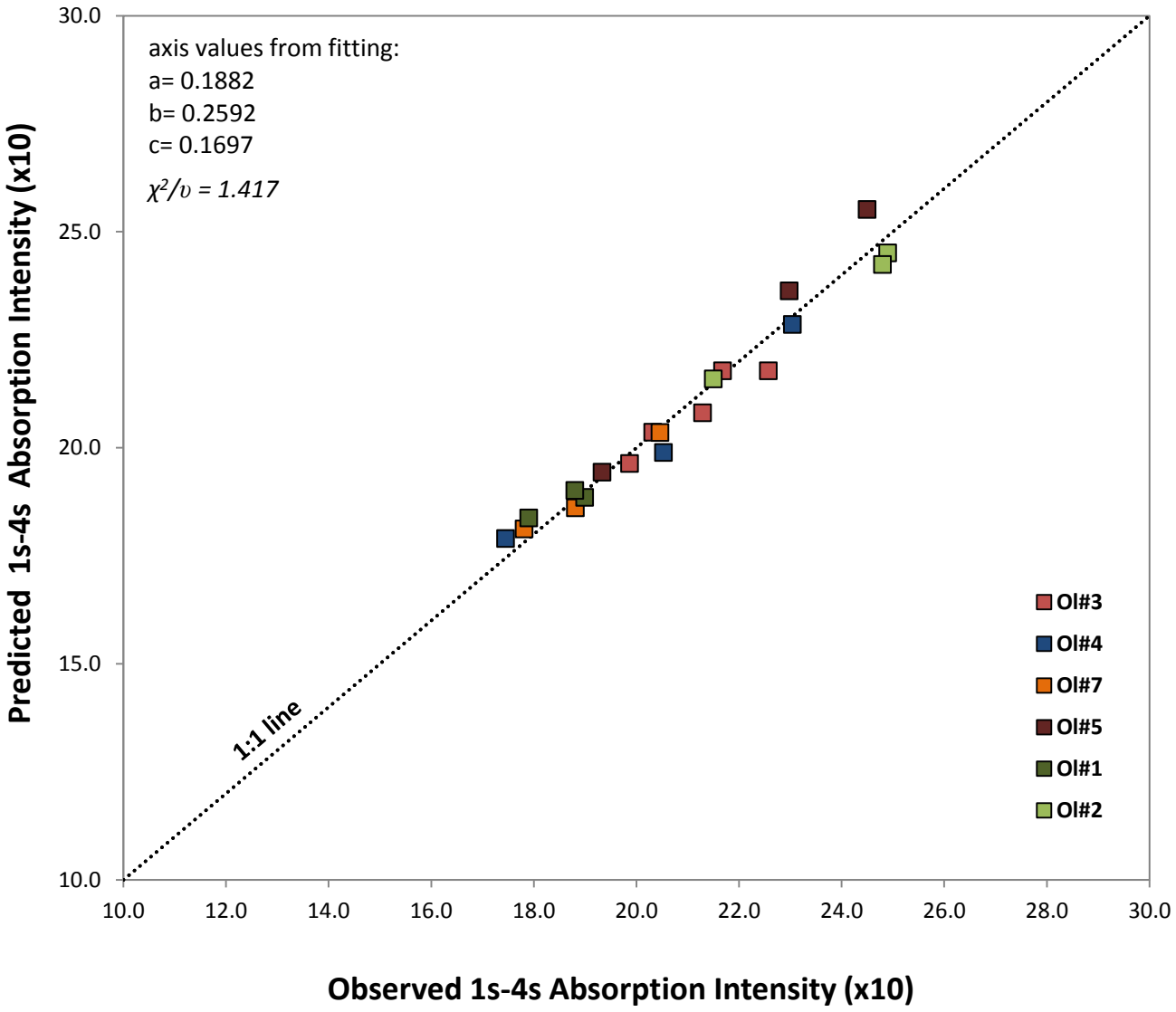

Figure 7 Shows the results of the "x-ray absorption indicatrix" fitting for the oriented olivine spectra. The plot shows a comparison of the predicted absorption cast as function of the angles θ and ϕ versus the actual measured absorption values for a suite of olivine crystals. The colors of the data points on the plot represent data from different individual olivine crystals.

This is a preprint, the final version is subject to change, of the American Mineralogist (MSA)
Cite as Authors (Year) Title. American Mineralogist, in press.
(DOI will not work until issue is live.) DOI: http://dx.doi.org/10.2138/am-2017-5911

Figure 8

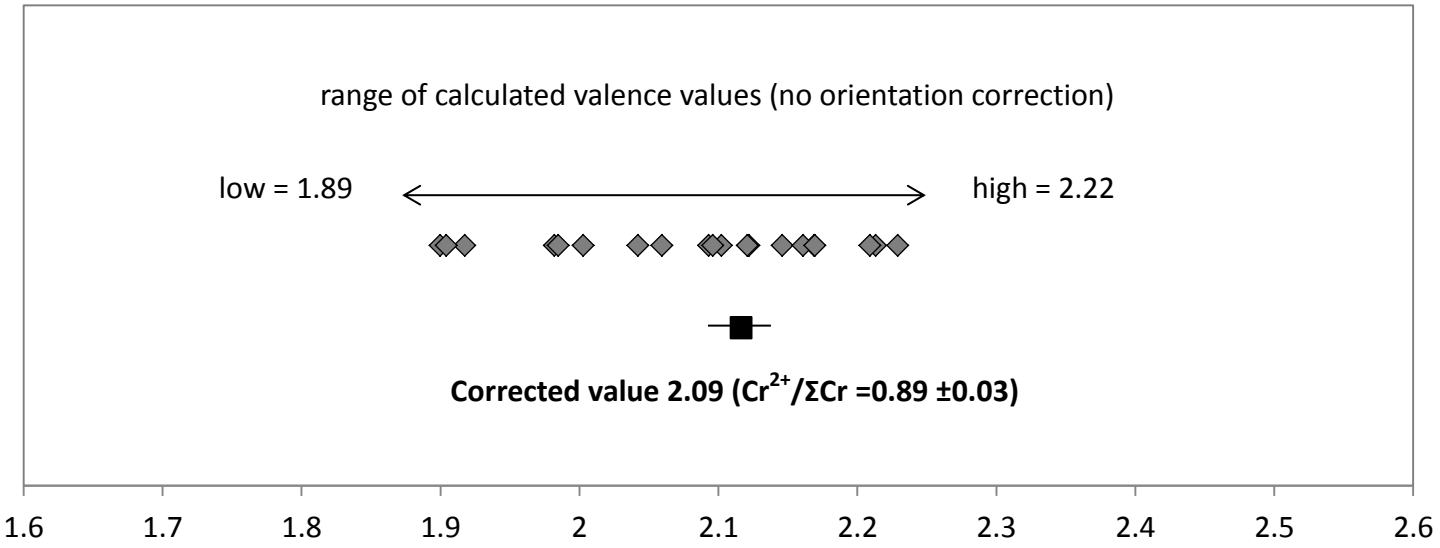

Figure 8. Illustrates the dispersion in the calculated Cr valence values of the suite of olivine crystals from ADF#4; the data show the effects of uncorrected anisotropy on the apparent Cr valence values. The orientation corrected Cr valence for the experimental olivine crystals is plotted in black below the observed range.

This is a preprint, the final version is subject to change, of the American Mineralogist (MSA)
Cite as Authors (Year) Title. American Mineralogist, in press.
(DOI will not work until issue is live.) DOI: http://dx.doi.org/10.2138/am-2017-5911

Table 1

Sample/Phase	SiO_2	Al_2O_3	CaO	MgO	Cr_2O_3	Total
ADF#4 oliv	43.23	0.16	0.44	56.10	0.35	100.55
1σ	*0.15*	*0.04*	*0.01*	*0.39*	*0.02*	*0.38*
ADF#4 glass	47.37	20.10	18.10	14.17	0.52	100.89
1σ	*0.23*	*0.12*	*0.09*	*0.09*	*0.02*	*0.35*
CMAS glass	58.74	13.64	24.71	2.64	0.28	100.01
1σ	*0.58*	*0.34*	*0.61*	*0.31*	*0.03*	*0.60*

This is a preprint, the final version is subject to change, of the American Mineralogist (MSA)
Cite as Authors (Year) Title. American Mineralogist, in press.
(DOI will not work until issue is live.) DOI: http://dx.doi.org/10.2138/am-2017-5911

Table 2

Olivine #	θ	ϕ	1s-4s intensity (x10)	Model Predicted (x10)	Residual
1_0	18	67	18.99	18.84	0.15
1_45	13	81	18.80	19.00	-0.20
1_90	11	59	17.90	18.37	-0.47
2_0	71	82	24.90	24.50	0.40
2_45	82	72	24.80	24.23	0.57
2_90	69	59	21.51	21.59	-0.09
3_0	47	89	22.57	21.78	0.79
3_0 repeat	47	89	21.68	21.78	-0.10
3_45	57	59	21.29	20.80	0.49
3_90	90	42	19.87	19.63	0.24
3_135	52	58	20.32	20.35	-0.03
4_0	55	87	23.04	22.85	0.19
4_45	42	60	20.53	19.89	0.64
4_90	7	47	17.45	17.89	-0.44
5_0	58	46	19.33	19.43	-0.10
5_45	76	70	22.98	23.63	-0.65
5_90	79	90	24.50	25.51	-1.01
7_45	27	53	18.81	18.60	0.21
7_90	66	51	20.46	20.35	0.11
7_0	13	51	17.81	18.12	-0.31